

Electronic Supplementary Information

CoAl-layered double hydroxide nanosheets as an active matrix to anchor amorphous MoS_x catalyst for efficient visible light hydrogen evolution

Shixiong Min^{*a} Jianhua Hou,^a Yonggang Lei,^a Xiangyu Liu,^a Yanan Li,^a Yuan Xue,^a

Entian Cui,^b Wenjun Yan,^c Wanxiu Hai^a and Fang Wang^a

^a *School of Chemistry and Chemical Engineering, Key Laboratory of Electrochemical
8 Energy Conversion Technology and Application, North Minzu University, Yinchuan,
750021, Ningxia Province, P. R. China.*

^b *Key Laboratory for Advanced Technology in Environmental Protection of Jiangsu
Province, Yancheng Institute of Technology, Yancheng, 224051, P. R. China.*

^c *Analytical Instrumentation Center, Institute of Coal Chemistry, Chinese Academy of
Sciences, Taiyuan 030001, P. R. China.*

**Corresponding author: E-mail: sxmin@nwnu.edu.cn.*

1. Experimental

1.1 Synthesis of bulk Co-Al LDH, Ni-Al LDH, Mg-Al LDH, and Zn-Al LDH.

1.1.1 Bulk Co-Al LDH: A wet reflux process based on the urea hydrolysis was used to synthesize the bulk Co-Al LDH (CO_3^{2-}) crystal.¹ In a typical procedure, calculated amount of $\text{CoCl}_2 \cdot 6\text{H}_2\text{O}$, $\text{AlCl}_3 \cdot 6\text{H}_2\text{O}$, and urea were dissolved into 1 L of deionized water in a three-neck round-bottom flask to give the final concentrations of 10, 5, 34 mM, respectively. The mixed solution was refluxed at 97 °C for 2 days under continuous magnetic stirring and protection of N_2 atmosphere. The resulting pink product was collected by filtration, washed with deionized water and then anhydrous ethanol in sequence, and dried at room temperature. Finally, the pink powder of bulk Co-Al LDH (CO_3^{2-}) crystal was obtained.

1.1.2 Bulk Ni-Al LDH: A hydrothermal process based on the urea hydrolysis was used to synthesize the bulk Ni-Al LDH (CO_3^{2-}) crystal.² In a typical procedure, calculated amount of $\text{NiCl}_2 \cdot 6\text{H}_2\text{O}$, $\text{AlCl}_3 \cdot 6\text{H}_2\text{O}$, and urea were dissolved into 100 mL of deionized water in a beaker to give the final concentrations of 10, 5, 15 mM, respectively. The mixed solution was then transferred into to a stainless-steel Teflon-lined autoclave. After being kept in a pre-heated oven at 190 °C for 2 days, the autoclave was cooled down naturally to room temperature. The green product was collected by centrifugation at 3000 rpm for 10 min. After being washed with washed with deionized water and then anhydrous ethanol in sequence, and dried at room temperature. Finally, the bulk Ni-Al LDH (CO_3^{2-}) crystal was obtained.

1.1.3 Bulk Mg-Al LDH: The bulk Mg-Al LDH (CO_3^{2-}) crystal was synthesized through a hydrothermal process based on the hexamethylenetetramine hydrolysis.³ In a typical procedure, calculated amount of $\text{MgCl}_2 \cdot 6\text{H}_2\text{O}$, $\text{AlCl}_3 \cdot 6\text{H}_2\text{O}$, and hexamethylenetetramine were dissolved into 100 mL of deionized water in a beaker to give a final concentrations of 20, 10, and 26 mM, respectively. Then, the mixed solution was transferred into to a stainless-steel Teflon-lined autoclave. After being kept in a pre-heated oven at 140 °C for 1 day, the product was collected by

centrifugation at 3000 rpm for 10 min. After being washed with washed with deionized water and then anhydrous ethanol in sequence, and dried at room temperature. Finally, the bulk white Mg-Al LDH (CO_3^{2-}) crystal was obtained.

1.2 Anion exchange reactions¹

The anion exchange reaction was carried out in a solution containing an excess of anions (Cl^- or NO_3^-) used to exchange the CO_3^{2-} in the bulk LDH (CO_3^{2-}) crystals, i.e. Co-Al LDH (CO_3^{2-}), Ni-Al LDH (CO_3^{2-}), and Mg-Al LDH (CO_3^{2-}). To obtain the LDH (Cl) crystals, i.e. Co-Al LDH (Cl), Ni-Al LDH (Cl), and Mg-Al LDH (Cl), 1.0 g of LDH (CO_3^{2-}) crystal was dispersed into 1000 mL of N_2 -purged aqueous solution containing 1.0 M of NaCl and 3.3 mM of HCl. Then, the aforementioned solution was sonicated for 3 min and mechanically stirred under N_2 for 24 h. The LDH (Cl) crystal was filtered, washed with deionized water and then anhydrous ethanol, and finally dried at room temperature. To obtain the LDH (NO_3^-) crystals, i.e. Co-Al LDH (NO_3^-), Ni-Al LDH (NO_3^-), and Mg-Al LDH (NO_3^-), the prepared LDH (Cl) crystal (0.5 g) was dispersed into 500 mL of N_2 -purged aqueous solution containing 1.0 M of NaNO_3 . Then, the aforementioned solution was sonicated for 3 min and mechanically stirred under N_2 for 24 h. The LDH (NO_3^-) crystals were filtered, washed with deionized water and then anhydrous ethanol, and finally dried at room temperature.

1.3 Exfoliation of bulk LDH crystals into LDH nanosheets (LDH NSs)

To obtain the LDH nanosheets, i.e. Co-Al NSs, Ni-Al NSs, and Mg-Al NSs, the prepared LDH (NO_3^-) crystal (100 mg) was dispersed into 100 mL of N_2 -purged formamide. Then, the aforementioned solution was sonicated for 10 min and agitated in a mechanical shaker at 160 rpm for 2 days. Then, the obtained transparent colloid solution containing LDH nanosheets (LDH NSs) (1 mg mL^{-1}) was directly used for following experiments.

1.4 In-situ photochemical preparation of LDH NSs/ MoS_x and photocatalytic H_2 evolution experiments.

In situ photochemical preparation of LDH NSs supported MoS_x catalysts and photocatalytic hydrogen evolution reactions were performed in an Erythrosine B-TEOA molecular system. Typically, Erythrosine B (0.5 mM), exfoliated LDH NSs in formamide (5 mL), and (NH₄)₂MoS₄ (100 μM) were added to a quartz reaction cell containing 100 mL of 15 vol% TEOA aqueous solution under vigorous stirring. For the preparation of unsupported MoS_x catalyst, the exact same synthesis procedure was employed without addition of any LDH NSs. The reaction solution was thoroughly degassed by repeated evacuation-N₂ filling, and finally refilled with N₂ to reach ambient pressure. After that, the reaction solution was irradiated by a 300 W Xe lamp (CEL-HXF300) equipped with an optical cut-off filter ($\lambda \geq 420$ nm). During the reaction, the mixture solution was continuously stirred and kept at a constant temperature by a cold-water jacket. The amount of H₂ produced was manually taken out by a gas-tight syringe (Agilent, 1.0 mL) and analyzed at given time intervals with a precalibrated gas chromatography (Tech comp; GC-7890II) with a thermal conductivity detector, a 5 Å molecular sieve column (3 mm×3 m), and with N₂ as carrying gas. The apparent quantum efficiency (AQE) was measured under the same photocatalytic reaction conditions with irradiation light through a band-pass filter of 420 nm. The photon flux of incident light was determined using a Ray virtual radiation actinometer (ApogeeMQ-500, silicon ray detector, light spectrum, 389–692 nm; measurement range, 0–4000 μmol m⁻² s⁻¹).

1.5 Characterizations

Transmission electron microscopy (TEM) and high-resolution TEM (HRTEM) images were taken with a HITACHI 7700 and FEI Talos F200s field emission transmission electron microscope. X-ray diffraction (XRD) patterns were investigated with a Rigaku B/Max-RB diffractometer with a nickel filtrated Cu K α radiation. X-ray photoelectron spectroscopy (XPS) measurements of the samples were performed on a K-Alpha surface analysis (Thermo Scientific) using X-ray monochromatization. The thickness of CoAl-NSs was measured by the tapping mode AFM (Bruker dimension ICON). UV–vis absorption spectra were taken with a TU-1810 UV-vis

spectrophotometer (Beijing Persee).

2. Additional figures

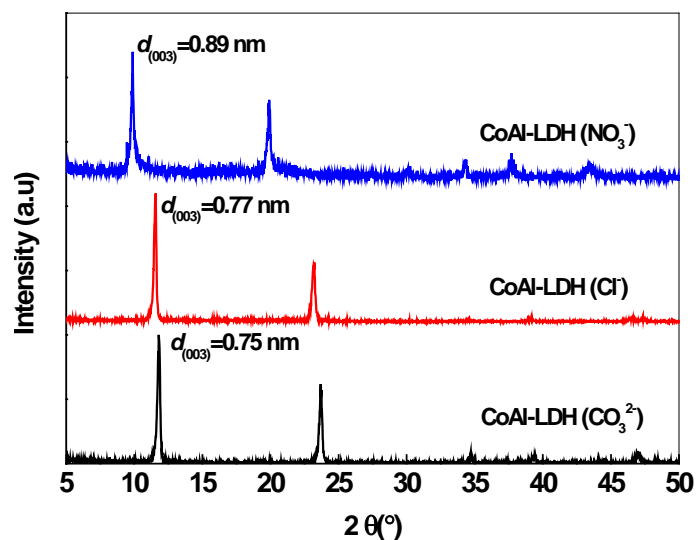


Fig. S1 XRD patterns of CoAl-LDH (CO_3^{2-}), CoAl-LDH (Cl^-), and CoAl-LDH (NO_3^-).

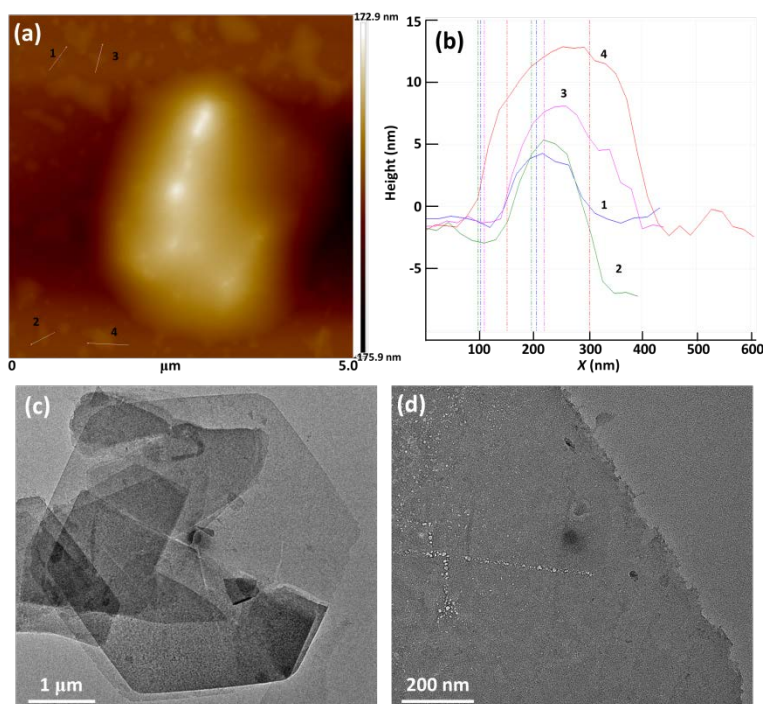


Fig. S2 (a) AFM images and (b) corresponding height profiles of CoAl-NSs. The thickness of CoAl-NSs is in the range of 12 to 30 nm. (c, d) TEM images of CoAl-NSs.

Fig. S2a and b show the AFM images and corresponding height profiles of

CoAl-NSs, revealing that the thickness of CoAl-NSs is in the range of 5 to 12 nm, which is much thicker than that of single-layer CoAl-NSs (~ 0.8 nm)⁴. This is probably due to the aggregations of CoAl-NSs during the sample preparation for the AFM analysis. Fig. S2c and d show the TEM images of CoAl-NSs at different magnifications, from which it can be seen that the individual CoAl-NS is transparent. These results clearly suggest the ultrathin nature of CoAl-NSs.

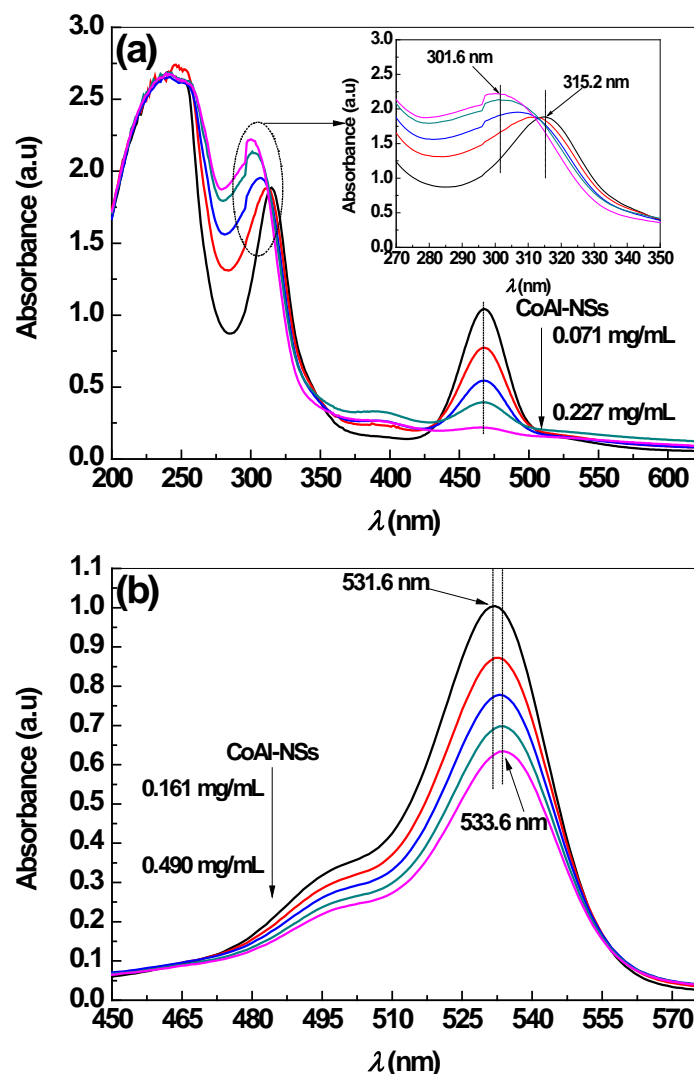


Fig. S3 (a) UV-vis absorption spectra of $(\text{NH}_4)_2\text{MoS}_4$ -TEOA solution in the presence of different concentrations of CoAl-NSs. (b) UV-vis absorption spectra of ErB-TEOA solution in the presence of different concentrations of CoAl-NSs.

The formation of $\text{ErB}/\text{CoAl-NSs}/[\text{MoS}_4]^{2-}$ assembly driven by electrostatic forces was also monitored by UV-vis absorption analysis, as shown in Fig. S3. Fig. S3a shows that the characteristic absorption peak of $[\text{MoS}_4]^{2-}$ obviously blue-shift from

315.2 to 301.6 nm with increasing concentration of the CoAl-NSs, clearly demonstrating that there is a strong interaction between positively charged CoAl-NSs and negatively charged $[\text{MoS}_4]^{2-}$. Fig. S3b shows that the characteristic absorption peak of ErB at 531.6 nm also red-shifts to 533.6 nm after adding CoAl-NSs. These results indicate that the ErB, $[\text{MoS}_4]^{2-}$, and CoAl-NSs could form an integrated assembly upon mixing. In the following light irradiation reaction, the $[\text{MoS}_4]^{2-}$ ions adsorbed on CoAl-NSs could be efficiently reduced to be MoS_x by the electrons from excited adsorbed ErB, forming CoAl-NSs/ MoS_x catalyst that will catalyze H_2 evolution reaction in the same system.

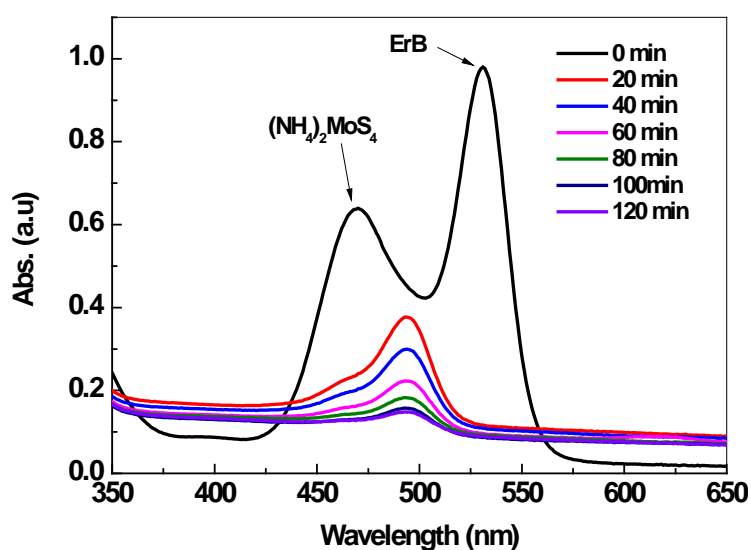


Fig. S4 Time-dependent UV-vis absorption spectra of ErB degradation during the photocatalytic H_2 reaction under visible light irradiation.

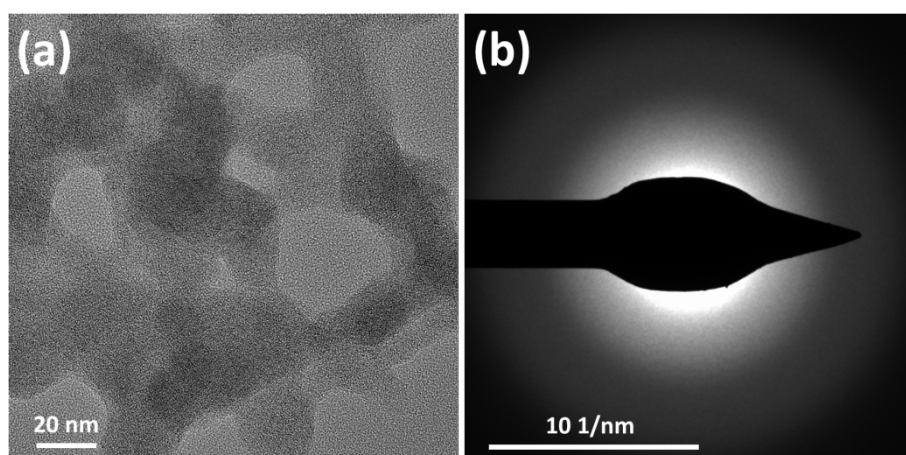


Fig. S5 (a) HRTEM image and (b) corresponding SAED pattern of anchored MoS_x nanoparticles on CoAl-NSs for CoAl NSs/ MoS_x catalyst.

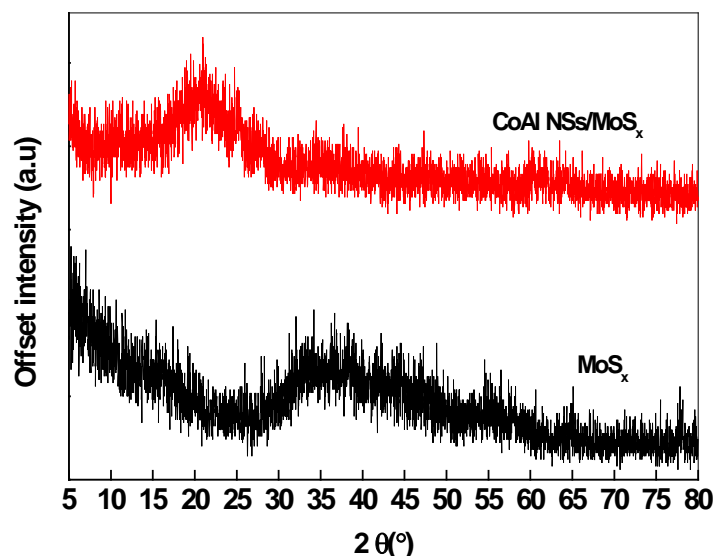


Fig. S6 XRD patterns of CoAl NSs/MoS_x and free MoS_x.

Fig. S5a shows the HRTEM image of anchored MoS_x nanoparticles on CoAl-NSs, no obvious lattice or Moiré fringes could be observed, suggesting that the anchored MoS_x nanoparticles are amorphous, which was further confirmed by the lack of any diffraction spots or rings in its corresponding SAED pattern (Fig. S5b) and characteristic diffraction peaks in its XRD pattern (Fig. S6).

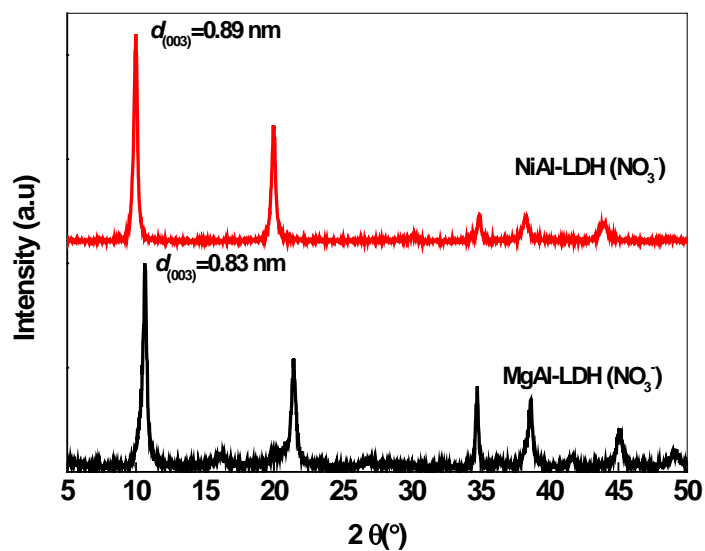


Fig. S7 XRD patterns of MgAl-LDH (NO₃⁻) and NiAl-LDH (NO₃⁻).

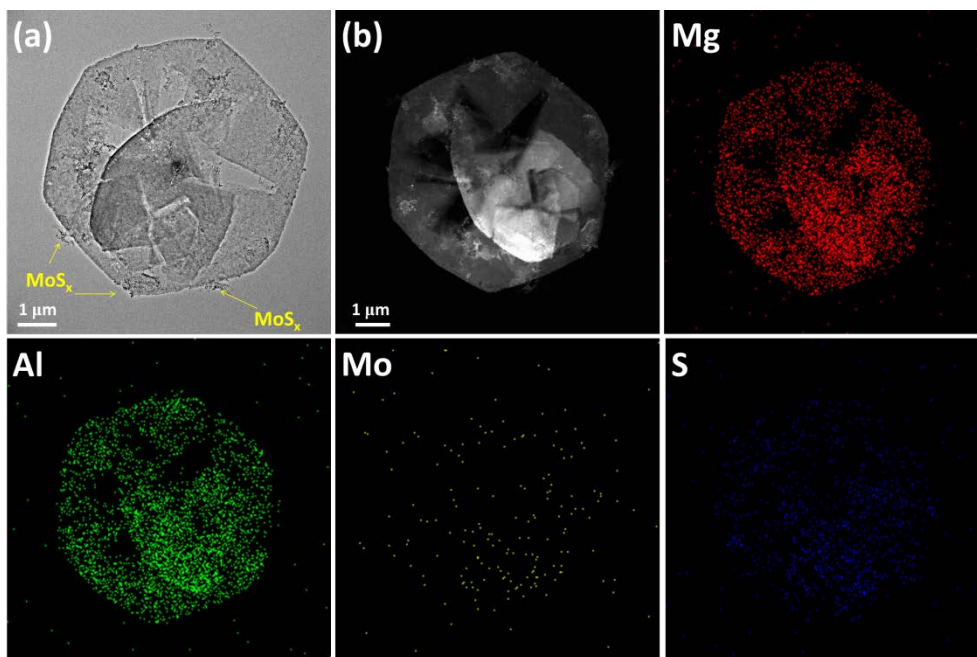


Fig. S8 (a) TEM image, (b) HAADF-STEM image, and corresponding Mg, Al, Mo, and S element mappings of MgAl-NSs/MoS_x catalyst.

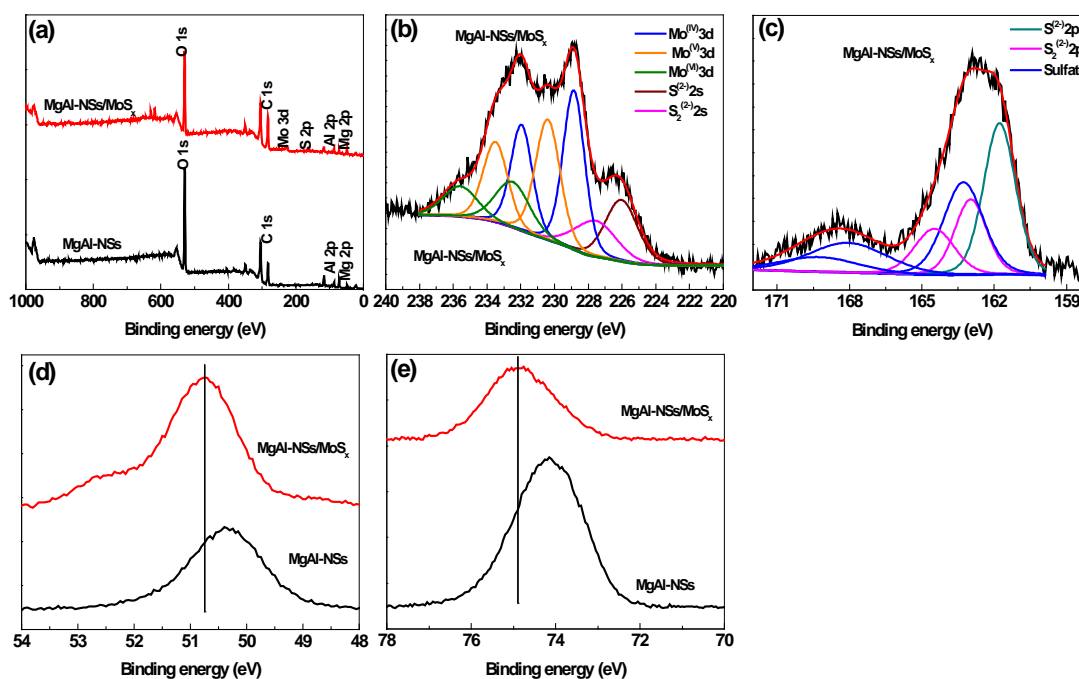


Fig. S9 (a) Survey XPS spectra of MgAl-NSs and MgAl-NSs/MoS_x. (b) Mo 3d and (c) S 2p core level XPS spectra of MgAl-NSs/MoS_x. (d) Mg 2p and (e) Al 2p core level XPS spectra of MgAl-NSs and MgAl-NSs/MoS_x.

Fig. S8 shows the TEM, HAADF-STEM images and corresponding EDS mapping of MgAl-NSs/MoS_x catalyst, revealing that only few number of MoS_x nanoparticles were grown on the edges and planes of MgAl-NSs, suggesting the MgAl-NSs is poor

support for the anchoring of MoS_x . Fig. S9 shows the XPS spectra of MgAl-NSs and MgAl-NSs/ MoS_x . From Fig. S9a-c, it can be seen that MoS_x can be grown on the surface of MgAl-NSs with the existing states similar to that of MoS_x grown on CoAl-NSs. Fig. S9d and e show that the binding energies for Mg 2p and Al 2p of MgAl-NSs slightly shifted to the higher values after loading of MoS_x , but there are no new peaks associated to the formation of “MgMoS” or “AlMoS”. Distinct with CoAl-NSs, the accessible and coordinatively unsaturated Mg and Al sites on MgAl-NSs are ineffective to form a “MgMoS” or “AlMoS” phase probably due to the instability of “Mg-S” and “Al-S” bonds that will hydrolyze quickly under reaction conditions. Therefore, when MgAl-NSs were used as support, the in-situ formed MoS_x nanoparticles cannot achieve a high dispersion due to their isolation from MgAl-NSs along with no formation of additional active sites like “CoMoS”, thus the resulting MgAl-NSs/ MoS_x show the low H_2 evolution activity.

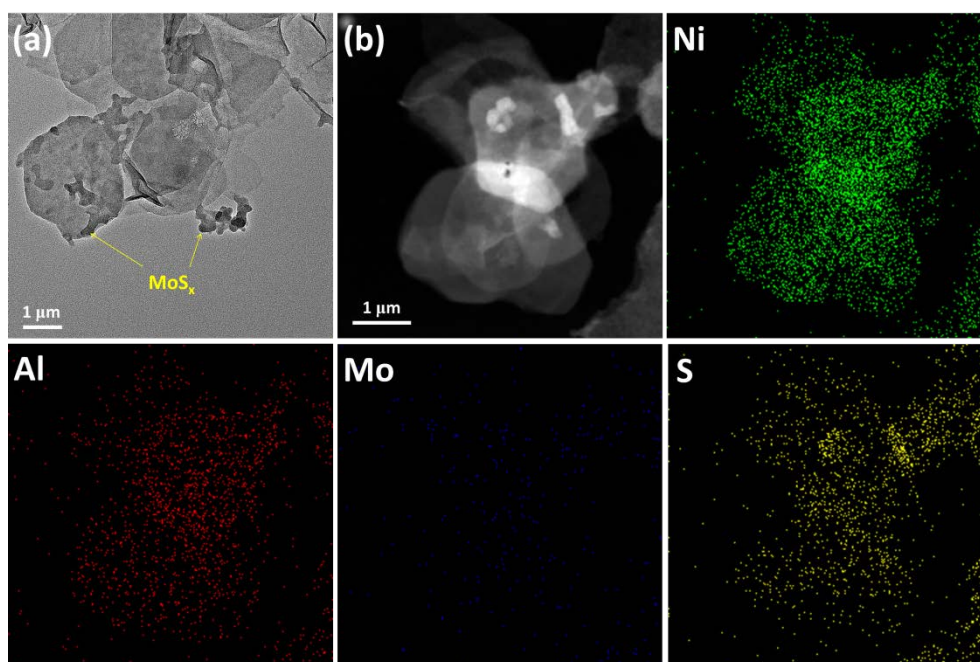


Fig. S10 (a) TEM image, (b) HAADF-SEM image, and corresponding Ni, Al, Mo, and S element mappings of NiAl-NSs/ MoS_x catalyst.

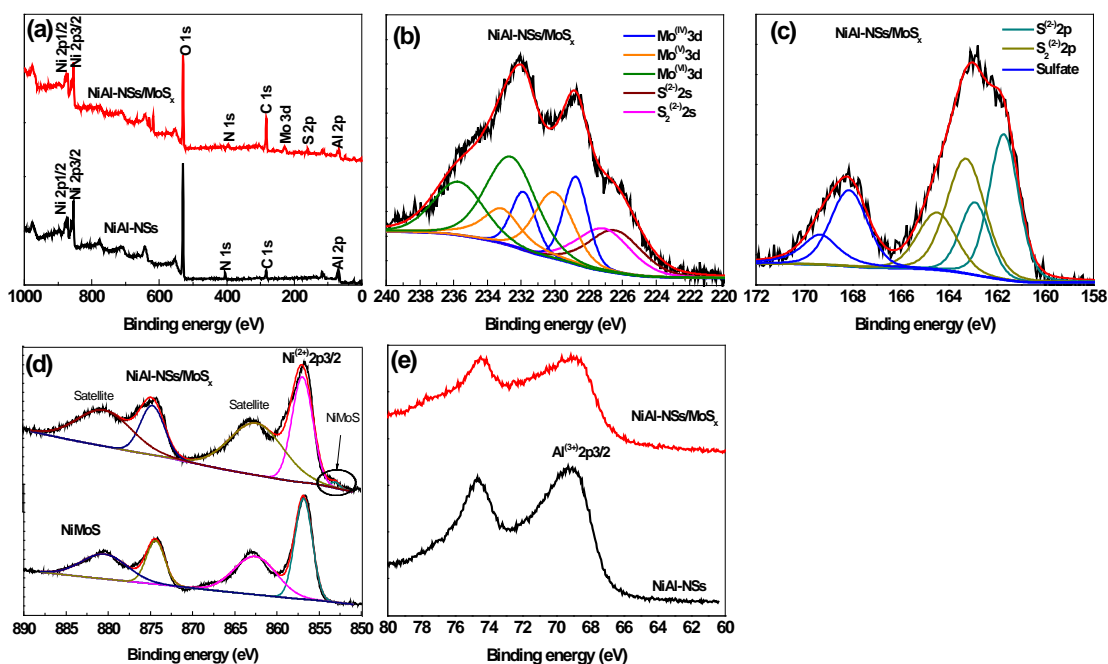


Fig. S11 (a) Survey XPS spectra of NiAl-NSs and NiAl-NSs/MoS_x. (b) Mo 3d and (c) S 2p core level XPS spectra of NiAl-NSs/MoS_x. (d) Ni 2p and (e) Al 2p core level XPS spectra of NiAl-NSs and NiAl-NSs/MoS_x.

Fig. S10 shows the TEM, HAADF-STEM images and corresponding EDS mapping of NiAl-NSs/MoS_x catalyst. Compared with CoAl-NSs as support, only large MoS_x particles with a size about 500 nm and MoS_x thin film could be observed on the surface of NiAl-NSs, thus the formed MoS_x catalyst with limited number of exposed active sites exhibits lower H₂ evolution activity. The XPS results in Fig. S11a-c show that the MoS_x can also be loaded on NiAl-NSs to form NiAl-NSs/MoS_x catalyst. Compared with the NiAl-NSs, the Ni 2p XPS spectrum (Fig. S11d) of NiAl-NSs/MoS_x catalyst shows a new and small peak at 852.97 eV, which might be ascribed to the formation of “NiMoS” phase, while the Al 2p spectra of NiAl-NSs and NiAl-NSs/MoS_x catalyst are the same (Fig. S11e). These results suggest the coordinatively unsaturated Ni sites on NiAl-NSs can form a strong interaction with MoS_x during the photoreduction of [MoS₄]²⁻, however, the formation of “NiMoS” is not effective to reducing the size of the anchored MoS_x catalyst as compared to the formation of “CoMoS” in CoAl-NSs/MoS_x catalyst. Thus, as to the NiAl-NSs/MoS_x catalyst, the in-situ formed MoS_x nanoparticles also cannot achieve a reduced size and high dispersion and the number of active “NiMoS” sites is limited, thus resulting in a

low H₂ evolution activity. In addition, it has been previously demonstrated that the modification of S-edges of MoS_x with Co doping is more effective than that with Ni doping because the Co-binding S-edges showed the lowest Gibbs free energy of adsorbed atomic hydrogen, ΔG_H , among various transition metal-binding S-edges, as a result, Co-promoted MoS_x catalyst shall have the highest H₂ evolution activity. This hypothesis has been extensively verified in electrocatalytic H₂ evolution reactions by using various transition-metal promoted amorphous MoS_x catalysts. Therefore, for the present works, it should be reasonable to see that the CoAl-NSs as support outperform NiAl-NSs for anchoring MoS_x nanoparticles for enhancing H₂ evolution performances.

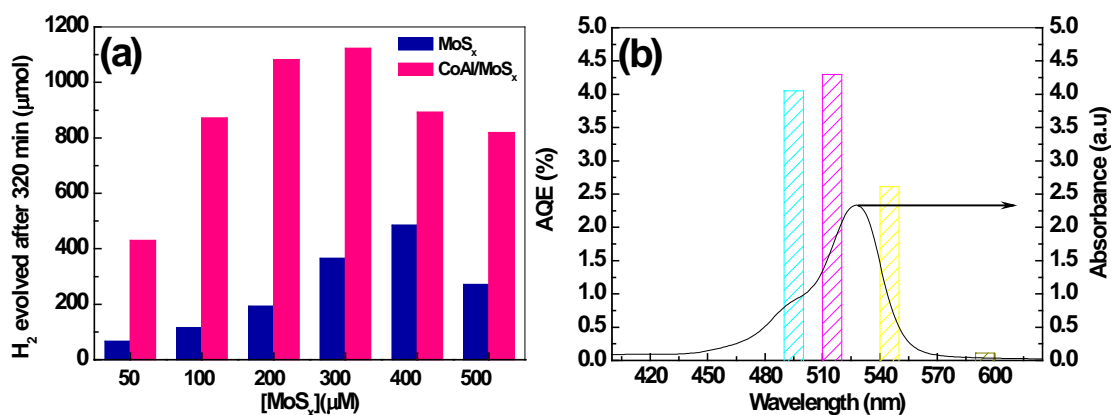


Fig.12 (a) Variations of H₂ evolution from ErB sensitized MoS_x and CoAl-NSs/MoS_x catalysts at different MoS_x concentrations. Reaction time, 320 min (b) The dependence of AQE for H₂ evolution over ErB sensitized CoAl-NSs/MoS_x catalyst on the wavelength of incident light and the absorption spectrum of ErB, where the concentration of MoS_x is 100 μM. Reaction conditions: CoAl-NSs, 5 mg; ErB, 0.5 mM; 100 mL TEOA solution; light source, Xe lamp (300 W), ≥ 420 nm.

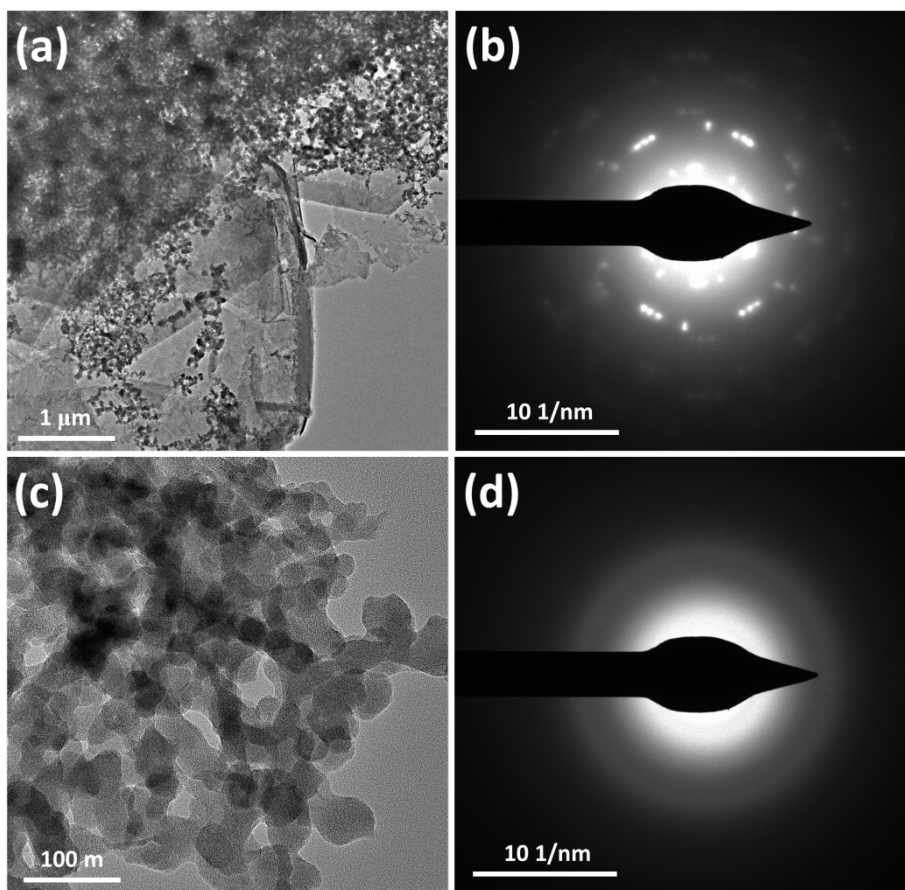


Fig. S13 (a) TEM image and (b) corresponding SAED pattern of CoAl-NSs/MoS_x catalyst prepared with a (NH₄)₂MoS₄ concentration of 500 μM. (c) HRTEM image of anchored MoS_x and (d) its corresponding SAED pattern, showing the MoS_x are aggregated and amorphous.

Fig. S13 shows the TEM and HRTEM images of CoAl-NSs/MoS_x catalyst prepared at (NH₄)₂MoS₄ concentration of 500 μM. It could be clearly observed that large amount of MoS_x nanoparticles aggregated on the surface of CoAl-NSs, which will lead to a shading effect for dye adsorption and light absorption. On the other hand, the severe aggregation of MoS_x nanoparticles on CoAl-NS can greatly block the exposure of for both intrinsic active sites of MoS_x and in-situ formed CoMoS active sites, thereby resulting in a decreased activity for H₂ evolution over CoAl-NSs/MoS_x catalyst.

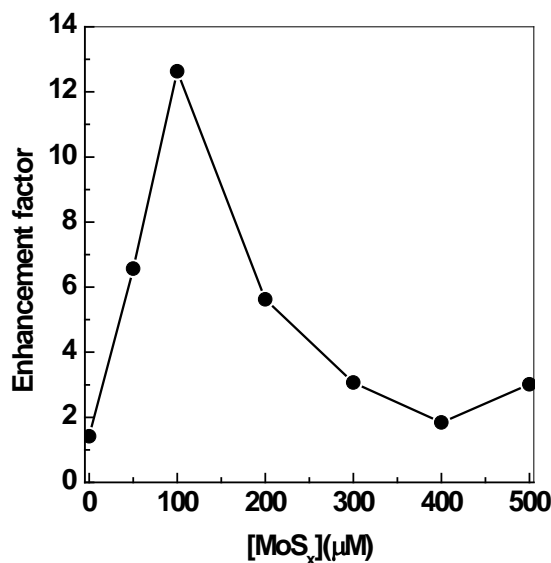


Fig. S14 Enhancement factor of H₂ evolution from ErB sensitized CoAl-NSs/MoS_x catalyst as compared to ErB sensitized MoS_x catalyst at different concentrations of MoS_x. Reaction conditions: CoAl-NSs, 5 mg; ErB, 0.5 mM; 100 mL TEOA solution; light source, Xe lamp (300 W), ≥420 nm.

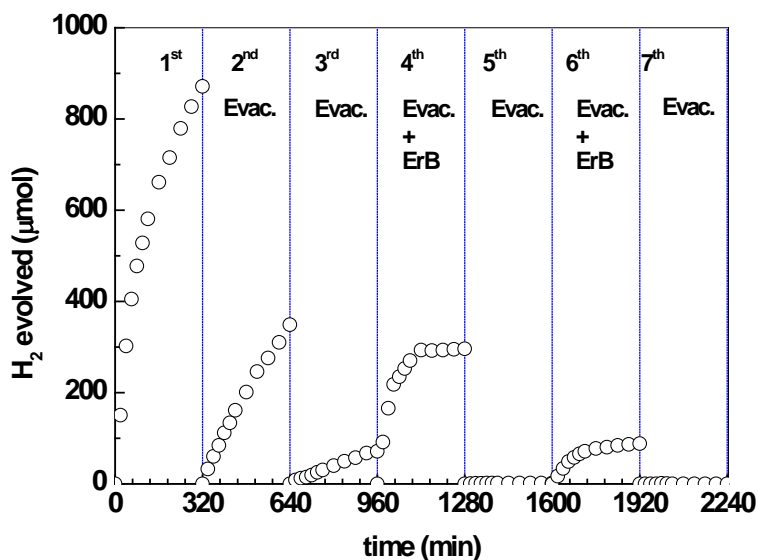


Fig. S15 Stability test of ErB sensitized CoAl-NSs/MoS_x catalyst for H₂ evolution. Reaction conditions: CoAl-NSs, 5 mg; ErB, 0.5 mM; MoS_x, 100 μM, 100 mL TEOA solution; light source, Xe lamp (300 W), ≥420 nm. In the first three runs, the system was evacuated only at the end of each run and directly subjected to light irradiation for next run.

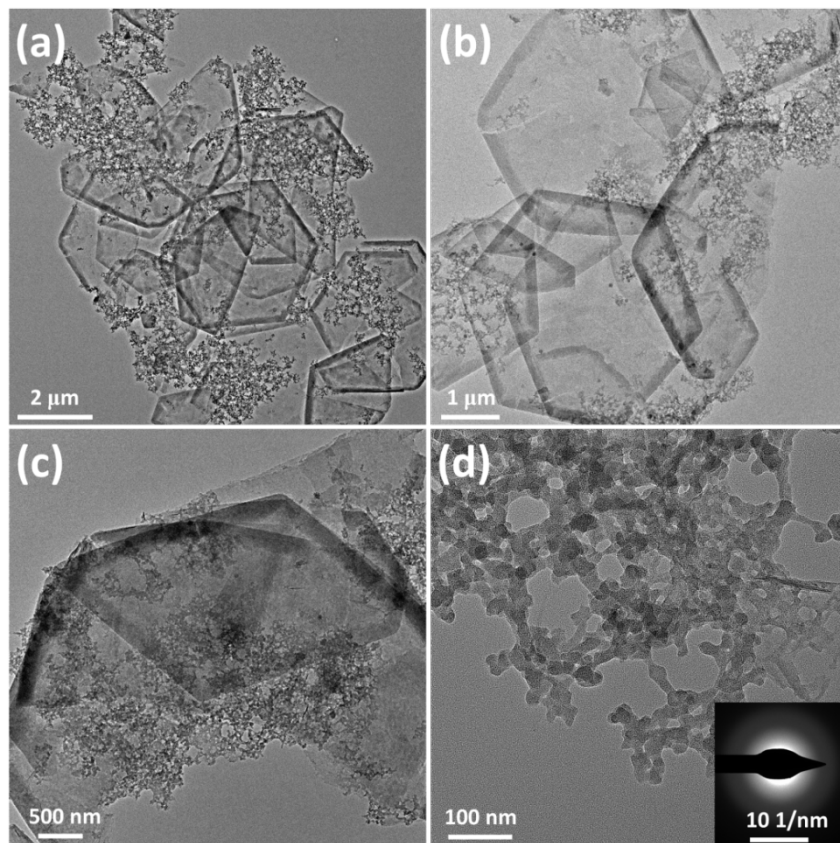


Fig. S16 (a-c) TEM images of CoAl-NSs/MoS_x catalyst after stability test. (d) HRTEM image of anchored MoS_x and corresponding SAED pattern.

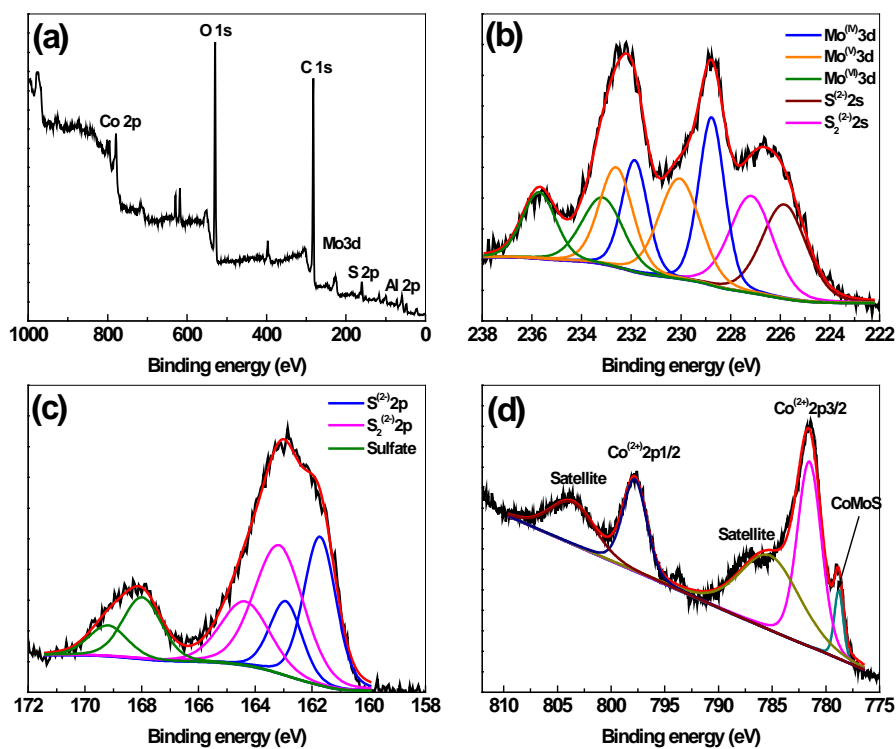


Fig. S17 Survey (a) and high-resolution XPS core level spectra of (b) Mo 3d, (c) S 2p, and (d) Co 2p for CoAl-NSs/MoS_x catalyst after stability test.

Fig. S16 shows the TEM and HRTEM images of CoAl-NSs/MoS_x catalyst after long-term stability test (Fig. S15). It can be clearly seen that most of the anchored MoS_x nanoparticles have peeled off from the CoAl-NSs surface and formed a number of larger aggregations after long-term use, which may account for the observed decrease in activity due to the reduce in exposed active sites. Fig. S17 show the XPS spectra of used CoAl-NSs/MoS_x catalyst, which revealed that the existing state of MoS_x nanoparticles and the surface bonding state of MoS_x to the CoAl-NSs have not changed significantly as compared to that of CoAl-NSs/MoS_x catalyst after 320 min reaction (Fig. 3f-h). The “CoMoS” phase at 778.8 eV still can be observed in the Co 2p XPS spectrum of the CoAl-NSs/MoS_x catalyst after long-term stability test, indicating that the interaction between anchored MoS_x and CoAl-NSs is strong, which ensures the CoAl-NSs/MoS_x catalyst with relatively good stability for H₂ evolution, as reflected by its H₂ evolution activity in the first three runs (Fig. S15), albeit with a decrease in activity due to the degradation of ErB (Fig. S4). It should be mentioned that the CoAl-NSs/MoS_x catalyst has not been separated from reaction solution, thus the decrease in activity in the following runs could probably be attributed to the accumulation of degraded dye species that not only are inactive for light absorption but also can absorb on the catalyst to block the active sites for H₂ evolution reaction, thus eventually leading to the deactivation of catalyst.

References

- [1] Z. Liu, R. Ma, M. Osada, N. Iyi, Y. Ebina, K. Takada and T. Sasaki, *J. Am. Chem. Soc.*, 2006, **128**, 4872.
- [2] Z. Liu, R. Ma, Y. Ebina, N. Iyi, K. Takada and T. Sasaki, *Langmuir* 2007, **23**, 861.
- [3] L. Li, R. Ma, Y. Ebina, N. Iyi and T. Sasaki, *Chem. Mater.*, 2005, **17**, 4386.
- [4] J. Ping, Y. Wang, Q. Lu, B. Chen, J. Chen, Y. Huang, Q. Ma, C. Tan, J. Yang, X. Cao, Z. Wang, J. Wu, Y. Ying and H. Zhang, *Adv. Mater.*, 2016, **28**, 7640.